Reverse Mapping of Coarse-Grained Polyethylene Chains from the Second Nearest Neighbor Diamond Lattice to an Atomistic Model in Continuous Space

Pemra Doruker and Wayne L. Mattice*

Institute of Polymer Science, The University of Akron, Akron, Ohio 44325-3909

Received March 4, 1997; Revised Manuscript Received June 25, 1997[⊗]

ABSTRACT: A high coordination lattice was recently introduced for the simulation of coarse-grained rotational isomeric state (RIS) model chains. This second nearest neighbor diamond (2nnd) lattice is formed by connecting every other site on a tetrahedral lattice. Monte Carlo simulations of polyethylene (PE) melts have recently been performed on the 2nnd lattice by incorporating the intramolecular short range interactions from the RIS model and the long range interactions using a potential derived from an averaging procedure of the Mayer function in the expansion for the second virial coefficient. In the present work, the reverse mapping of specific snapshots from the coarse-grained PE melt back to the fully atomistic representation in continuous space is demonstrated. Reverse mapping is, essentially, determining the location of intermediate backbone atoms that are not represented on the 2nnd lattice but exist on the diamond lattice. In certain situations, the new locations of two intermediate atoms may coincide, leading to an unrealistic local conformation with infinite energy. Although these collapse situations are rare in the case of PE, they still present a problem in finding an energetically acceptable snapshot, which can be further subject to energy minimization in continuous space. These local collapse phenomena can be avoided by taking into consideration the geometry of the underlying tetrahedral lattice during coarse-grained simulations. Consequently, specific snapshots from bulk PE simulations are reverse mapped and their energy is minimized. The cohesive energy densities of these energy-minimized snapshots are very close to the experimental values reported in the literature.

Introduction

Fully atomistic simulations in continuous space are not feasible for studying most of the dynamic processes in polymeric systems, which have large characteristic sizes and long relaxation times, such as the equilibration of melts and the healing of interfaces. Monte Carlo (MC) simulations on lattices offer an advantage in this respect by discretizing the phase space and utilizing fast integer algorithms.

Our approach is to replace the direct route (single dashed arrow) between replicas I and IV in Figure 1 by an alternative path (three solid arrows) in order to obtain a trajectory that is long enough to analyze the slower relaxational processes such as chain diffusion in polymers melts. This alternative path consists of three steps: (i) mapping of an atomistic system onto a coarse-grained representation on a sparsely occupied high coordination lattice (I → II), (ii) performing MC simulations on the high coordination lattice (II → III), and (iii) reverse mapping of selected snapshots from the high coordination lattice back to an atomistic system (III → IV).

If desired, energy minimization of these reverse-mapped snapshots can be rapidly performed, thereby generating an off-lattice replica in continuous space.

The high-coordination lattice introduced for this purpose permits the mapping of polymer chains for which the bond angles are approximately tetrahedral, with torsion angles near 180° and ±60°.[1,2] This lattice is formed by connecting every other site on the tetrahedral lattice. Thus, it is called the second nearest neighbor diamond lattice or 2nnd lattice, for short. It has a coordination number of 12. Since the tetrahedral lattice easily accommodates the rotational isomeric state (RIS) model for polyethylene (PE), its coarse-grained derivative—the 2nnd lattice—also accommodates PE, as a single chain or at bulk density.[2,3] The coarse-grained derivative retains only half of the carbon atoms, one for each CH_2CH_2 unit. Then $C_{2i}H_{4i+2}$ is represented by i sites on the 2nnd lattice. This approach yields a lattice on which only 15−20% of the sites are occupied at the experimental densities for PE melts. The low occupancy of the 2nnd lattice contributes to the efficiency of the simulation in step ii.

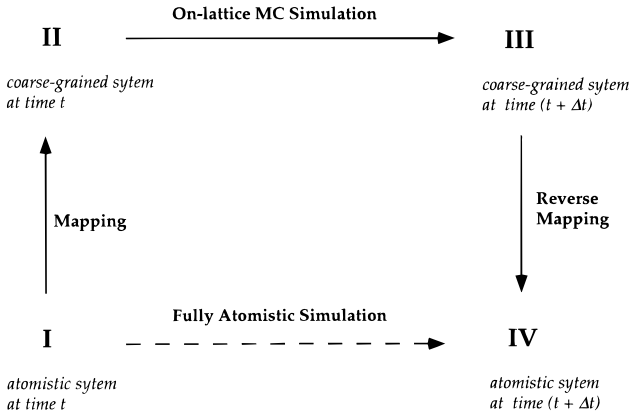

Figure 1. Schematic representation of the route (three solid arrows) taken to perform Monte Carlo simulations on a coarse-grained high-coordination lattice in order to produce replicas at a longer Δt than is accessible directly by fully atomistic simulations (single dashed arrow).

The RIS model[4,5] is used to incorporate short range conformational characteristics of specific polymers into the MC simulations, so that detailed information on the local chain conformations can be obtained from the trajectories. Long range intramolecular interactions and intermolecular interactions are also included to mimic the cohesive nature of polymer systems.[3]

Steps i and ii have been established in previous work for PE[2] and poly(oxyethylene) (POE)[6] as isolated chains

[⊗] Abstract published in *Advance ACS Abstracts,* August 15, 1997.

S0024-9297(97)00297-0 CCC: $14.00

under θ conditions and for PE in the melt.[3] In this work, we will describe the reverse mapping procedure (step iii) for PE and discuss the solution of the problems associated with it. In our case, reverse mapping means determining the coordinates of intermediate backbone atoms, which are ignored on the coarse-grained 2nnd lattice. The representation of $C_{2i}H_{4i+2}$ by i sites on the 2nnd lattice is thereby replaced by a representation with $2i - 1$ sites on the tetrahedral lattice, from which the 2nnd lattice originates. (The cyclic polyethylene, $C_{2i}H_{4i}$, is represented by i sites on the 2nnd lattice, and introduction of the intermediate methylene groups produces $2i$ sites on the 2nnd lattice.) Subsequent attachment of a methyl group at one end of the acyclic chain produces a representation with $2i$ sites. From this point on, it is trivial to place the hydrogen atoms on the internal methylene groups and terminal methyl groups in the case of PE, if we further want to carry out fully atomistic simulations. Coarse-grained conformations on the 2nnd lattice can be uniquely reverse mapped back to the tetrahedral lattice. However, some overlapping of the intermediate backbone atoms, "collapsed beads", is encountered in rare (but identifiable) local environments. Although these local environments occur with very low probability in PE melts, they are almost certain to occur in individual replicas in the simulation of a very large system. If not dealt with properly, the large repulsive energy of these rare locations will severely compromise the energetic analysis of reverse-mapped replicas.

In the following section, a brief description of the simulation parameters for PE will be given with reference to earlier work on the 2nnd lattice simulations. The reverse-mapping procedure will also be addressed. In the Results and Discussion, the problem of collapsed beads during the reverse mapping and its solution will be explained together with simulation results.

Model and Method

The Two Lattices. Figure 2a gives an illustration of a $3 \times 3 \times 3$ section of the 2nnd lattice, which is composed of every other site on a diamond lattice. It is equivalent to the closest packing of uniform hard spheres. In the present context, the name "2nnd" is preferred over "closest packing of hard spheres", because it conveys more accurately the relationship of the lattice to the preferred conformations of PE. The twelve nearest neighbors of the central bead are connected to it by bold lines on the figure. The 2nnd unit cell is a slanted cubic cell. Therefore, the lattice sites can be indicated by integer numbers. If the axes passing through the slanted sites of the 2nnd lattice are denoted by x', y', and z', the angle between any two of the x', y', and z' axes is 60°. On the figure, the Cartesian xy plane and the 2nnd $x'y'$ plane are the same and the bisector of the angle between the x' and y' axes is collinear with the bisector of the angle between the x and y axes. There are eight complete unit cells in this figure, with two cells in each of the x', y', and z' directions.

At any stage of the simulation, the chains on the 2nnd lattice can be reverse mapped back to the tetrahedral lattice. Figure 2b illustrates the tetrahedral lattice, on which the coarse-grained 2nnd lattice sites are made distinct by the larger, dark gray spheres. If the small open spheres and their connections are deleted and the nearest neighbor larger spheres are connected, the 2nnd lattice in Figure 2a is obtained with a slightly different point of view. The smaller, white beads on the diamond

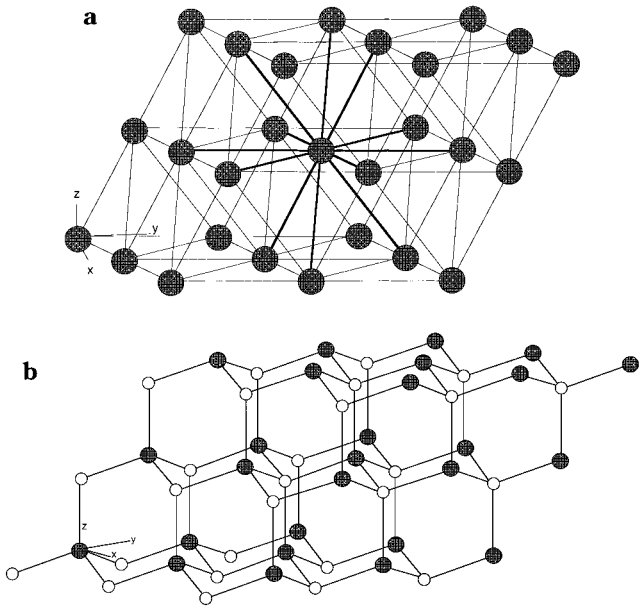

Figure 2. (a) Representation of a $3 \times 3 \times 3$ section of the 2nnd lattice. The bonds that connect the middle bead to its 12 nearest neighbors are highlighted with bold lines. (b) Representation of the tetrahedral lattice, from which the 2nnd lattice originates. Here, the larger, dark spheres are retained on the 2nnd lattice sites, but the white spheres are deleted. (If only the dark spheres are connected, the lattice in (a) is obtained, with a slightly different point of view.)

lattice represent the intermediate beads that are ignored on the 2nnd lattice due to coarse graining. After the simulations are run with i beads on the 2nnd lattice, the reverse mapping of any snapshot of PE back to the tetrahedral lattice is basically determining the location of the small, white spheres in Figure 2b, which are occupied by $i - 1$ methylene units if the chain is linear and i methylene groups if the chain is cyclic. The location of each intermediate white bead between any two large spheres is unique, once it is determined whether the vectors connecting the big and the small beads, which are collinear with the z axis, point in the $+$ or $-$ z-direction. A terminal methyl group can be added in any of six positions (three at each end) for the acyclic chain.

Energetics. The short range interactions are implemented through the RIS formalism by using an extended statistical weight matrix to determine the probabilities of the different states on the 2nnd lattice. There are four distinct states on the 2nnd lattice, differentiated from one another by the length of the segment connecting beads i and $i + 2$, which corresponds to four bonds with two torsional angles on the tetrahedral lattice. Equivalently stated, beads i and $i + 2$ on the 2nnd lattice are analogous to methyl groups in *n*-pentane, with bead $i + 1$ being the central methylene group. The four distances between methyl groups in *n*-pentane are found in the *tt*, *tg*, g^+g^+, and g^+g^- conformations. Since there are three states (*trans* (*t*), *gauche*$^+$ (g^+) and *gauche*$^-$ (g^-)) for each torsion angle of PE in the RIS model, several pairs of torsional states on the tetrahedral lattice correspond to the same state on the 2nnd lattice. The ($i \rightarrow i + 2$) segment length on the 2nnd lattice runs from 2.5 to 5 Å for PE. The segment length of 2.5 Å, which is the lattice spacing between first neighbors, corresponds to the ($i \rightarrow i + 2$) segment length in the g^+g^- or g^-g^+ torsional states on the tetrahedral lattice. The length of 5 Å for ($i \rightarrow i + 2$) corresponds to the extended conformation of *tt* torsional

Table 1. Changes in the Conformation of the Atomistic Model on the Tetrahedral Lattice That Move a Single Bead in the 2nnd Lattice Representation, without Disturbing Any of the Other Beads

change[a]	degeneracy[b]	moving C atoms	changing torsions
$ttg^+tt \rightarrow g^+tg^-tg^+$	4	2	3
$ttg^+tg^+ \rightarrow g^+tg^-tg^-$ [c]	8	2	3
$ttg^+tg^- \rightarrow g^+tg^-tt$	4	2	3
$g^+tg^+tg^+ \rightarrow g^-tg^-tg^-$	2	2	3
$ttg^+g^+t \rightarrow g^+tg^-g^-g^-$	8	2	4
$ttg^+g^+g^+ \rightarrow g^+tg^-g^-t$	8	2	4
$ttg^+g^+g^- \rightarrow g^+tg^-g^-g^+$	8	2	4
$g^+tg^+g^+t \rightarrow g^-tg^-g^-g^-$ [d]	8	2	4
$g^+tg^+g^+g^- \rightarrow g^-tg^-g^-g^+$	4	2	4
$tg^+g^+g^+t \rightarrow g^-g^-g^-g^-g^-$	4	2	5
$tg^+g^+g^+g^+ \rightarrow g^-g^-g^-g^-t$	4	2	5
$tg^+g^+g^+g^- \rightarrow g^-g^-g^-g^-g^+$	8	2	5
$g^+g^-g^-g^+ \rightarrow g^-g^+g^+g^+g^-$ [e]	2	2	5
$ttg^+g^-tt \rightarrow g^-tg^-g^+tg^+$ [f]	4	3[g]	4[h]
$ttg^+g^-tg^+ \rightarrow g^-tg^-g^+tg^-$	8	3[g]	4[h]
$ttg^+g^-tg^- \rightarrow g^-tg^-g^+tt$	4	3[g]	4[h]
$g^+tg^-g^+tg^- \rightarrow g^-tg^+g^-tg^+$	2	3[g]	4[h]
$ttg^+g^+tt \rightarrow g^+g^+g^+g^+g^+$	4	3[g]	4[h]
$ttg^+g^+tg^+ \rightarrow g^+g^+g^+g^+g^-$	8	3[g]	4[h]
$ttg^+g^+tg^- \rightarrow g^+g^+g^+g^+$t	8	3[g]	4[h]
$ttg^+g^+g^+t \rightarrow g^+g^+g^+g^+tg^-$	8	3[g]	4[h]
$ttg^+g^+g^+g^+ \rightarrow g^+g^+g^+g^+tt$	4	3[g]	4[h]
$ttg^+g^+g^+g^- \rightarrow g^+g^+g^+g^+tg^+$	8	3[g]	4[h]
$tg^+g^+g^+tg^+ \rightarrow g^-tg^+g^+g^+g^-$	8	3[g]	4[h]
$tg^+g^+g^+tg^- \rightarrow g^-tg^+g^+g^+t$	4	3[g]	4[h]
$tg^+g^+g^+t \rightarrow g^-tg^+g^+tg^-$	4	3[g]	4[h]
$tg^+g^+g^+g^+g^- \rightarrow g^-tg^+g^+tg^+$	8	3[g]	4[h]
$g^+tg^+g^+tg^+ \rightarrow g^-g^+g^+g^+g^-$ [i]	4	3[g]	4[h]
$g^+tg^+g^+g^+g^- \rightarrow g^-g^+g^+g^+tg^+$	4	3[g]	4[h]
$ttg^+g^-g^+t \rightarrow g^-tg^-g^+g^-g^-$	8	3[g]	5
$ttg^+g^-g^+g^+ \rightarrow g^-tg^-g^+g^-t$ [j]	8	3[g]	5
$tg^+g^-g^+tg^- \rightarrow g^-g^-g^+g^-tg^+$	8	3[g]	5

[a] Mirror images, reverse sequences, and reverse changes are also permissible. [b] Sum, including mirror images, reverse sequences, and reverse changes. [c] The mirror image, $ttg^-tg^- \rightarrow g^-tg^+tg^+$, is depicted in (a) of Figure 3. [d] This conformational change is depicted in (b) of Figure 3. [e] This conformational change is depicted in (c) of Figure 3. [f] This conformational change is depicted in (a) of Figure 4. [g] The middle atom in this sequence of three consecutive atoms is the one that is represented on the 2nnd lattice. [h] The two sets with three moving atoms and four rotating bonds differ with regard to whether the rotating bonds are numbers 1, 2, 5, and 6 in the hextet or numbers 1, 3, 4, and 6 in the hextet. [i] The mirror image, $g^-tg^-g^-tg^- \rightarrow g^+g^-g^-g^-g^+$, is depicted in (b) of Figure 4. [j] The mirror image, $ttg^-g^+g^-g^- \rightarrow g^+tg^+g^-g^+t$ [l], is depicted in (c) of Figure 4.

states. Intermediate lengths are obtained in the *tg*, *gt*, g^+g^+, and g^-g^- states. For PE the first- and second-order interaction energy parameters of Abe et al.[7] are used to determine the statistical weights of the four distinguishable states on the 2nnd lattice. The procedure of determining the short range interactions in coarse-grained RIS chains on the 2nnd lattice has been described in detail.[2]

Parameters for the long range intramolecular interaction between lattice sites that are separated by more than two 2nnd bonds, as well as the intermolecular interactions, are derived for PE from the spherically isotropic Lennard Jones (LJ) interaction between ethylene units, since each lattice site accommodates two backbone atoms due to coarse graining. Self-avoidance and mutual avoidance are absolute. The second virial coefficient expression is used to determine average interaction energies among neighboring lattice sites. Average interaction energies for the first through fifth neighboring sites are calculated as 12.501, 0.084, −0.611, −0.137, and −0.036 kJ/mol, respectively, for PE at 170 °C (443 K).[3] Since the lattice spacing between first

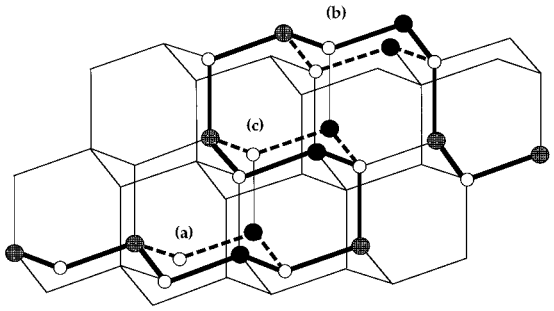

Figure 3. Representation of the local moves that change the coordinates of two consecutive carbon atoms in the atomistic representation on the diamond lattice, but only a single bead in the representation of the same changes on the 2nnd lattice. The bold continuous lines connect the carbon atoms in the chain in the initial conformation, and local portions move as shown by the bold dashed lines. The large black circles are the moving and stationary beads on the 2nnd lattice. The small open circles are the carbon atoms that are represented on the tetrahedral lattice but are ignored on the 2nnd lattice. Details on the conformations are in Table 1.

neighbors is 2.5 Å, which is less than the sum of the van der Waal's radii of two ethylenes, the first shell energy is highly repulsive. In the MC simulations reported here, we retain only the energies in the first through third neighboring sites, because the negative interactions in the fourth and higher neighboring sites are much weaker than the interaction in the third neighboring site. The details on the determination of long range interaction parameters and simulation results for bulk PE can be found in ref 3.

Elementary Moves. The MC moves that are applied on the 2nnd lattice are single bead moves. Each internal bead has either one, three, or no choices of different locations of movement, depending on the location of its two bonded neighbors. When viewed in the atomistic detail available on the underlying diamond lattice, there are 186 permissible moves for internal beads, enumerating all possible mirror images, reverse sequences, and reverse conformational changes. These 186 permissible moves fall naturally into six distinguishable types.

Three types of moves alter the position of two consecutive carbon atoms (but only one bead on the 2nnd lattice). When both the initial and final positions of these two carbon atoms are drawn simultaneously, they occupy positions 2, 3, 5, and 6 of a cyclohexane ring, with the chain extending from this ring at positions 1 and 4, as depicted in Figure 3. Here the bonds in the atomistic chain on the tetrahedral lattice are drawn with bold solid lines. The black (2nnd) and white (intermediate tetrahedral) spheres indicate the lattice sites, through which the chain passes. Three different moves are made on different parts of the chain. Dashed lines indicate the new bonds after the moves. The three cyclohexane rings are in the chair conformation, with the attachment of the main chain being diequatorial, equatorial−axial, or diaxial in (a), (b), and (c), respectively. Torsion angles change at three, four, or five C−C bonds in (a), (b), and (c), respectively, as summarized in Table 1.

The other three types of moves change the positions of three consecutive carbon atoms in the fully atomistic representation on the diamond lattice. Only the middle member of this triplet is retained on the 2nnd lattice. When both the initial and final positions of the triplet of carbon atoms are drawn simultaneously, they occupy positions 2−4 and 6−8 in a cyclooctane ring, with the

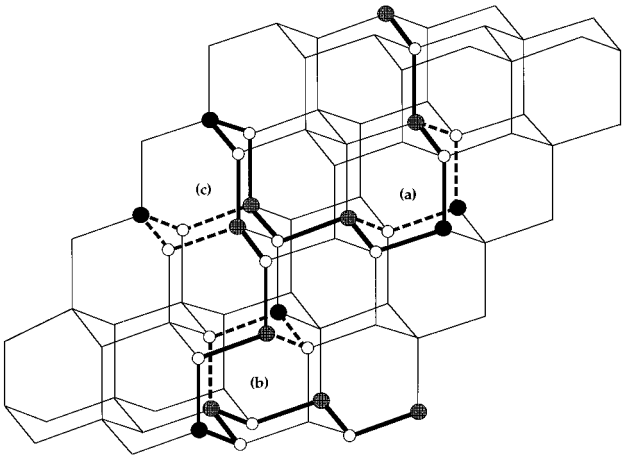

Figure 4. Representation of the local moves that change the coordinates of three consecutive carbon atoms in the atomistic representation on the diamond lattice, but just a single bead in the representation of the same changes on the 2nnd lattice, where only the middle atom in each triplet is retained. The bold continuous lines connect the carbon atoms in the chain in the initial conformation, and local portions move as shown by the bold dashed lines. The large black circles are the beads on the 2nnd lattice. The small open circles are the carbon atoms that are represented on the tetrahedral lattice but are ignored on the 2nnd lattice. Details are in Table 1.

chain extending from the ring at positions 1 and 5, as depicted in Figure 4. Details of the changes in the conformation of the atomistic chain are summarized in Table 1.

Occupancy. The occupancy of the lattice is quite low even at bulk conditions since each occupied lattice site represents two backbone atoms. For example, for bulk PE at 200 °C (25 chains of $C_{316}H_{634}$ at a density of 0.76 g/cm^3), the occupancy of the 2nnd lattice site is 18.0%, with each chain occupying 158 lattice sites. This low occupancy allows for efficient bulk simulations. The acceptance rates for $C_{100}H_{202}$ decrease by less than a factor of 2 when bulk simulations are compared with single chain simulations at 170 °C. The acceptance rate is 14% for $C_{100}H_{202}$ at a density of 0.75 g/cm^3.

Energy Minimization of Reverse-Mapped Snapshots. Energy minimization (EM) of reverse-mapped snapshots is performed by using software from MSI, Inc. The coordinates of the carbon atoms in the chains that have been reverse mapped back onto the tetrahedral lattice are read by Insight II, and the hydrogen atoms are added onto the backbone atoms by the Builder Module of Insight II. Then, energy minimization of the bulk snapshot is performed by using Discover 3.0 with the CVFF force field (version 2.3, no cross terms and no Morse potentials). The three stages of the EM procedure are summarized below:

1. Nonbonded potentials are scaled by 10^{-5} to avoid large conformational changes due to the initial close contacts among the hydrogen atoms. EM is performed till the gradient is less than 10 kcal/(mol Å).

2. Nonbonded potential scaling is reduced by a factor of 10, in four successive stages, to 10^{-1}. At each stage, EM is carried out till the gradient is less than 10 kcal/(mol Å).

3. Finally, nonbonded potential scaling is reduced to 1, i.e., no scaling. EM is performed till the gradient is less than 0.1 kcal/(mol Å).

In all steps, the steepest descents method is used if the gradient is greater than 1000 kcal/(mol Å), and conjugate gradient is used otherwise.

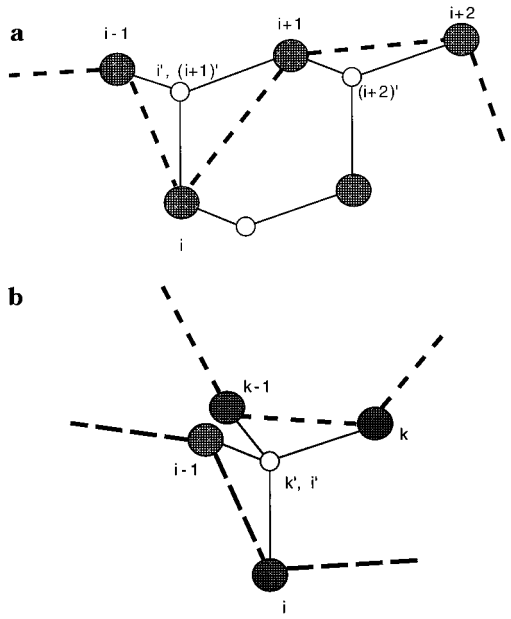

Figure 5. Unrealistic conformations that may arise during the reverse mapping of 2nnd chains back to the tetrahedral lattice. (a) Short range collapse of intermediate beads i' and $(i + 1)'$, which occurs as the chain locally folds back on itself during reverse mapping. (b) Long range collapse, which occurs if the intermediate beads k' and i' from two different chains or different parts of the same chain occupy the same site after reverse mapping. The four shaded spheres are at the apexes of a regular tetrahedron, and the open sphere is at their center of mass.

Results and Discussion

During the reverse mapping of chains, unrealistic conformations may arise when the new locations of two intermediate beads coincide on the tetrahedral lattice. These situations, which will be denoted as "collapsed beads" in the following discussion, are illustrated in Figure 5. On this figure, a small section of the lattice in Figure 2b is enlarged in order to better visualize these local collapse phenomena. There are two different cases of collapse, short range and long range, which are given by Figure 5a,b, respectively.

In Figure 5a, a portion of the 2nnd chain with three coarse-grained bonds is shown by dashed lines connecting the dark spheres (backbone atoms) running through beads $i - 1$ through $i + 2$. The chain folds back on itself between beads $i - 1$ and $i + 1$ when it is reverse mapped back to the tetrahedral lattice. If we denote by i' the intermediate bead on the tetrahedral lattice between beads $i - 1$ and i, then beads i' and $(i + 1)'$ coincide or collapse after reverse mapping. The state of the segment between $i - 1$ and $i + 1$ is weighted by the statistical weight of g^+g^- and g^-g^+ conformations in the simulations,[2] which is a small weight for PE due to the pentane effect.[7] Therefore, the occurrence of these conformations in bulk PE will be small. For example, in bulk PE simulations at 200 °C (25 chains of $C_{316}H_{634}$ with density of 0.76 g/cm^3) only 50 such collapses are observed on the average at each snapshot (∼2 collapsed beads per chain, with a minimum of 25 and maximum of 76 collapses in the snapshots examined). With 9 chains of $C_{100}H_{202}$ at a density of 0.75 g/cm^3 at 170 °C, 4−5 collapses are observed on the average at each snapshot (the range is 0−11 collapses in the snapshots examined). Although the fraction of the atoms in the local collapse phenomena is low, they still present a

problem because every collapse contributes a very large repulsive energy if it is not resolved. The density of polyethylene of high molecular weight is about 0.77 g/cm^3 at 170 °C,[7] but we use a slightly lower density for $C_{100}H_{202}$, based on an estimate using the value of 0.74 g/cm^3 for $C_{44}H_G$ at this temperature.[8]

The second collapse situation shown in Figure 5b may result from the long range interactions. Here, neighboring beads $i-1$, i and $k-1$, k belong to different chains or to different portions of the same chain. These four beads are mutually first neighbors on the lattice, where they form a cage with the intermediate beads i' and k' lying in the cage. Thus, the intermediate beads collapse. Although such a situation can be expected to arise during reverse mapping, it is extremely rare in reality, due to the high repulsive forces that exist between first neighbors (~12 kJ/mol). In such a situation, high repulsive interactions between first neighbors (i and $k-1$), (i and k), ($i-1$ and $k-1$), and ($i-1$ and k) would result in a locally unfavorable conformation. Thus, such a situation has not been observed in any of our bulk PE simulations to date.

To avoid the local collapse phenomena described by Figure 5a, three consecutive beads of the same chain should not occupy, at the same time, any three of the four sites around the cage, shown in Figure 5b. This restriction could be implemented into the simulations by specifying the pairs of base vectors that connect beads $i-1 \rightarrow i$ and $i \rightarrow i+1$, if beads $i-1$, i, and $i+1$ on the chain were to occupy three sites around the cage. These pairs of base vectors, which add up to 24 in total, are to be avoided during the simulation. Implementation of this restriction in the simulations does not decrease the acceptance rate significantly in bulk PE simulations (less than 1% decrease), because the occurrence of these restricted conformations was already very low due to the pentane effect. The application of this restriction has minimal effect on the CPU time of the simulations. (However, in polymers such as POE in which the occurrence of g^+g^- and g^-g^+ conformations is higher, the acceptance rate should drop significantly due to the application of this restriction. But, in POE the initial acceptance rate to start with is higher than that of PE.[6])

A second alternative is to run the bulk simulations without using this restriction. In that case, before reverse mapping any specific snapshots, it will be necessary to run a brief simulation for several MC steps with this restriction until these local collapses are extinguished and, then, the final conformation can be reverse mapped. We have, in fact, carried out this procedure with $C_{100}H_{202}$ simulations at 170 °C (9 chains of $C_{100}H_{202}$ with a density of 0.75 g/cm^3). It takes 10−140 Monte Carlo steps to eliminate all the collapses, depending on the specific snapshot. Figure 6a gives a snapshot from this simulation showing the coarse-grained chains on the 2nnd lattice. This specific snapshot contains 7 local collapses. Their locations are indicated by the numbers on the figure. Also, the beads $i-1$, i, and $i+1$ in each of these local regions, which lead to the collapse of beads i' and $(i+1)'$ (see Figure 5a), are highlighted in bold. A brief simulation of 10 Monte Carlo steps with the restriction is run to remove these collapses before reverse mapping. Then the energy of the fully atomistic reverse-mapped snapshot is minimized by the procedure given in the Model and Method section. The final snapshot after EM is illustrated in Figure 6b with a space-filling model, where the backbone carbons and the hydrogens are represented by the darker and lighter spheres, respectively.

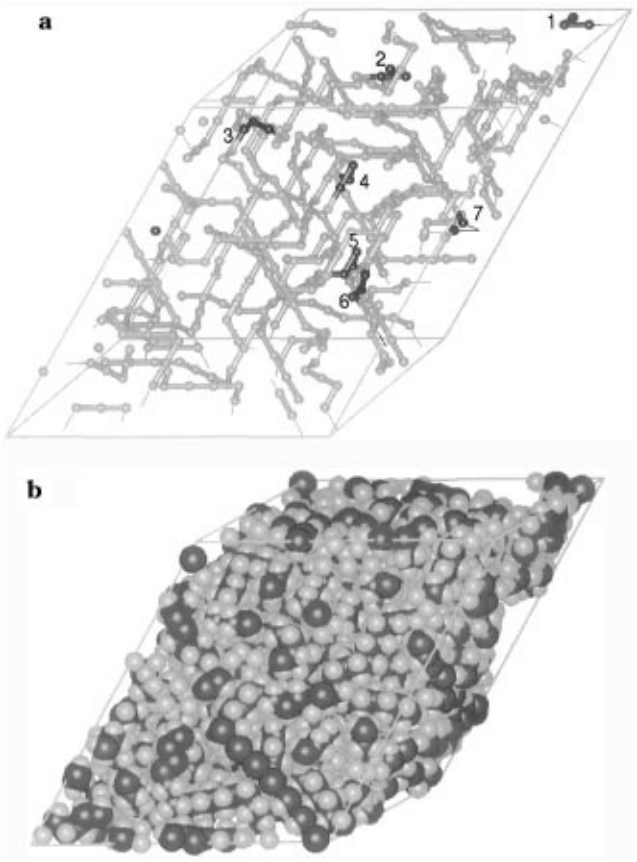

Figure 6. (a) Specific snapshot from the Monte Carlo simulation on the 2nnd lattice (9 chains of $C_{100}H_{202}$ at 170 °C). The snapshot contains seven local collapses, which are indicated by the darker beads and numbers on the figure. (b) The same snapshot after the collapses are removed and EM is performed on the fully atomistic reverse-mapped structure.

Distribution of Torsion Angles. After reverse mapping, but before EM, the distribution of torsion angles is limited to the three values, 180° and ±60°, that are allowed on the tetrahedral lattice. The populations at ±60° are nearly identical, as expected from the symmetry of the torsion potential energy function, and are smaller than the population at 180°, as expected from the form of the torsion potential energy function for *n*-butane.

During the EM, the torsion system moves off-lattice, and the δ functions at 180° and ±60° are replaced by continuous distributions. An example is illustrated in Figure 7, which was prepared using data for the system depicted in Figure 6. The heights of the δ functions were 0.624 at 180°, 0.179 at 60°, and 0.197 at −60°. The continuous distribution produced by EM maintains the strong preference for torsion angles near 180° and ±60°, with the highest population near 180°, and nearly equivalent populations near ±60°, as expected.[9] When averaged over ten independent snapshots, each having first been subjected to EM, the population of the t state is 0.617; its population is 0.609 for the specific snapshot depicted in Figure 7. The remaining population is nearly equally distributed between the two g states. The RIS model employed in the mapping procedure predicts 58.7% of the bonds are in t states at this temperature. The continuous distribution for the t state has its maximum very close to 180° and is nearly symmetrically distributed about the maximum. In contrast, the dis-

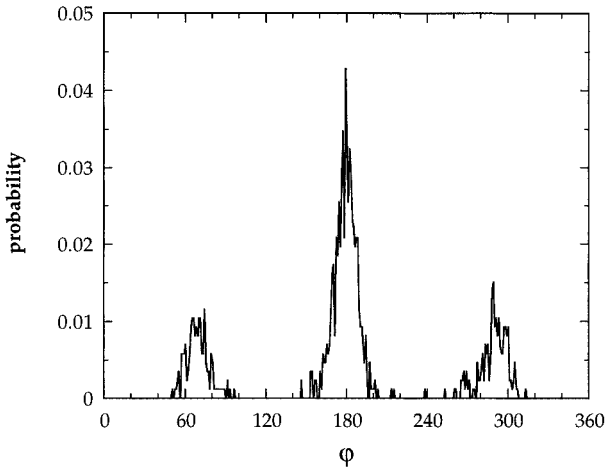

Figure 7. Distribution of the torsion angles in a representative snapshot after reverse mapping and subsequent EM, using the same snapshot as in Figure 6. The heights of the δ functions that represented the distribution before EM were 0.624, 0.179, and 0.197 at 180°, 60°, and −60°, respectively.

Table 2. Cohesive Energy Densities of Specific Snapshots on the 2nnd Lattice (before Reverse Mapping) and in Continuous Space (after Reverse Mapping and EM)

run[a]	density, g/cm^3	snapshot	no. of collapses	CED on 2nnd, cal/cm^3	CED after EM, cal/cm^3
I	0.75	1	0	26.2 (42.1)[b]	56.4
I	0.75	2	2	25.8 (41.7)	53.6
I[c]	0.75	3	7	25.2 (41.0)	55.1[d]
II	0.86	4	6	34.3 (55.1)	72.8
II	0.86	5	1	33.6 (54.4)	72.4
II	0.86	6	10	34.6 (55.1)	74.6

[a] Both runs are performed with 9 chains of $C_{100}H_{202}$ at 170 °C. Run I is performed in a box of 13 × 13 × 15 cells, corresponding to the estimated density of $C_{100}H_{202}$ at the specific temperature, whereas run II is performed in a box of 13 × 13 × 13, which gives the bulk density of amorphous PE at room temperature. [b] The numbers in parentheses include the contributions from the fourth and higher neighbors (see text). [c] This snapshot is the one used for Figures 6 and 7. [d] The number tabulated is for the structure produced by adding 49 carbon atoms by reverse mapping. Placement of an additional methyl group at the end of every chain changes this number to 55.2−55.8 cal/cm^3.

tributions in the *g* states have their maxima at $\pm(60° + \Delta\varphi)$ where $\Delta\varphi$ is roughly 10°. The direction and size of this displacement in the most probable torsion angle for a *g* state is in excellent agreement with the expectation from the RIS model for PE.[9] Therefore, the EM produces a reasonable minor adjustment in the coordinates, as judged by the distribution of the torsion angle, when it converts the system to an off-lattice representation.

In contrast to the accuracy in the estimation of the population of rotational isomeric states, there is a large statistical uncertainty in the mean square dimensions evaluated from the chains in a few snapshots subjected to EM. For example, the three snapshots listed in the first three lines in Table 2 contain a total of 27 chains, with squared end-to-end distances, r^2, ranging over nearly 2 orders of magnitude, from 47 to 2872 Å^2. A characteristic ratio of 6.7 would require $\langle r^2\rangle_0 = 1553$ Å^2; the average over the 27 chains in the three snapshots is 1216 Å^2. The ratio $\langle r^2\rangle/\langle s^2\rangle$ is 6.5 for these 27 chains, where s^2 denotes the squared radius of gyration. The mean square dimensions of the 27 chains increase slightly, by about 5%, during the energy minimization.

Cohesive Energy. Table 2 presents results from two independent simulations at 170 °C, each performed with 9 chains of $C_{100}H_{202}$. Run I is carried out at a density of 0.75 g/cm^3 (in a 13 × 13 × 15 simulation box), which is close to the experimental density of PE at 170 °C. Run II is performed at a higher density of 0.86 g/cm^3 (in a 13 × 13 × 13 simulation box), which approximates the density of a PE melt at room temperature. Three different snapshots are chosen from both runs. The three snapshots are separated by at least 500 000 MC steps. During such a time period, the centers of mass of the chains diffuse a distance of about two radii of gyration, on the average. Therefore, the snapshots are independent from each other. The number of local collapses occurring in each snapshot is tabulated. The cohesive energy density (CED) of the snapshots on the 2nnd lattice is calculated by using the long range interaction energies for the first, second, and third nonbonded neighbors on the lattice. The numbers for the CED in parentheses in Table 2 include the longer range interactions, with the assumption that the occupancy of the fourth and higher neighbors is identical with the overall occupancy of the entire system. Nearly equivalent numbers are obtained if the actual occupancies are used instead. The CED of reverse-mapped and energy-minimized snapshots are calculated by using the Amorphous Cell module of Insight II. In order to get reasonable (positive) CED values with the fully atomistic force fields, the snapshots should contain no collapses and EM should be performed to remove the close contacts among hydrogen atoms prior to CED calculations. The experimental cohesive energy of PE is reported to be in range 8.2−9.6 kJ/mol at room temperature,[10] which corresponds to a CED range of 60−70 cal/cm^3. Although the CED values calculated with the lattice energy parameters seem to be lower than the experimental values, the CED of reverse-mapped and energy-minimized snapshots from run II are very close to the experimental range.

Incorporation of a terminal methyl group onto every one of the chains in this simulation changes the CED by 1% or less.

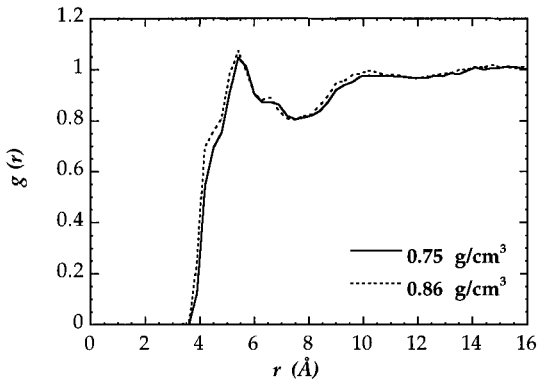

Figure 8. Intermolecular C−C pair distribution for $C_{100}H_{202}$ melts after reverse mapping and subsequent energy minimization.

Positional Order. The carbon−carbon intermolecular pair distribution function is plotted in Figure 8 for $C_{100}H_{202}$ at two densities. The curves are obtained by averaging the results of energy-minimized snapshots (10 snapshots at 0.75 g/cm^3, and 8 snapshots at 0.86 g/cm^3). Very similar results are obtained at these two densities. The positions and amplitudes of the first maximum and the first minimum are comparable to those obtained from a molecular dynamics simulation performed for a $C_{44}H_{90}$ melt at 400 K and a density of 0.76 g/cm^3.[8] The two kinks on the left- and right-hand side of the first

peak indicate a slight residual order that is not found in the simulation of Smith et al. However, the kink on the left-hand side does appear in the site−site intermolecular radial distribution function reported for polyethylene by Honnell et al.[11]

Acknowledgment. This work was supported by National Science Foundation grant DMR 95-23278.

References and Notes

(1) Rapold, R. F.; Mattice, W. L. *J. Chem. Soc., Faraday Trans.* **1995**, *91*, 2435.
(2) Rapold, R. F.; Mattice, W. L. *Macromolecules* **1996**, *29*, 2457.
(3) Cho, J.; Mattice, W. L. *Macromolecules* **1997**, *30*, 637.
(4) Flory, P. J. *Statistical Mechanics of Chain Molecules*; Wiley: New York, 1969.
(5) Mattice, W. L.; Suter, U. W. *Conformational Theory of Large Molecules. The Rotational Isomeric State Model in Macromolecular Systems*; Wiley: New York, 1994.
(6) Doruker, P.; Rapold, R. F.; Mattice, W. L. *J. Chem. Phys.* **1996**, *104*, 8742.
(7) Orwoll, R. A. In *Physical Properties of Polymers Handbook*; Mark, J. E., Ed.; AIP Press: Woodbury, NY, 1996; p 81.
(8) Smith, G. D.; Yoon, D. Y.; Zhu, W.; Ediger, M. D. *Macromolecules* **1994**, *27*, 5563.
(9) Abe, A.; Jernigan, R. L.; Flory, P. J. *J. Am. Chem. Soc.* **1966**, *88*, 631.
(10) van Krevelen, D. W. *Properties of Polymers. Their Estimation and Correlation with Chemical Structure*; Elsevier Science Publishers B.V.: Amsterdam, The Netherlands, 1990.
(11) Honnell, K. G.; McCoy, J. D.; Curro, J. G.; Schweizer, K. S.; Narten, A. H.; Habenschuss, A. *J. Chem. Phys.* **1991**, *94*, 4659.

MA970297U